

Article

Characteristic and Geological Implications of Major Elements and Rare Earth Elements of Triassic Chang 7 Oil Shale in Tongchuan City, Southern Ordos Basin (China)

Delu Li ^{1,*}, Rongxi Li ^{1,*}, Tao Xue ², Baoping Wang ³, Futian Liu ¹, Bangsheng Zhao ¹ and Di Zhao ¹

¹ School of Earth Sciences and Resources, Chang'an University, Xi'an 710054, China; zhaobs88@163.com (F.L.); zhaodi95@foxmail.com (B.Z.); d47zhao@uwaterloo.edu.ca (D.Z.)

² No.2 Geo-Exploration Institute, Henan Provincial Bureau of Geo-Exploration and Mineral Development, Zhengzhou 450000, China; james_alice@foxmail.com

³ Yanchang Oilfield Co., Ltd., Yan'an 716000, China; Davidhappyday@foxmail.com

* Correspondence: lidelu322@126.com (D.L.); rongxi99@163.com (R.L.)

Received: 19 February 2018; Accepted: 9 April 2018; Published: 12 April 2018



Abstract: The study of the oil shale from Triassic Chang 7 oil layer in Ordos Basin is of great importance to oil and gas resources investigation. Based on systematic analyses of major elements and rare earth elements of twelve oil shale samples and grain size analyses of four sandstone samples from the Yishicun Profile in southern Ordos Basin, the elements characteristics and corresponding geological implications are discussed. The Al/Si and Si/(Si + Al + Fe) of oil shale samples are in small range, with the averages of 0.29 and 0.67, indicating that quartz is the main mineral and the oil shale deposits near terrigenous provenance. Rare earth elements of the oil shale illustrate the enrichment of light rare earth elements (LREEs) and deficit of heavy rare earth elements (HREEs). The Chondrite- and North American shale composite (NASC)-normalized distributing patterns manifested that the oil shale have been derived from the same terrigenous source and controlled by a similar sedimentary environment. The vertical variation of major elements and REEs show that the heterogeneity of oil shale samples is relatively low. By grain size analysis, the interlayer sandstone is the typical turbidite. The Chemical index of alteration (CIA) and (Fe + Mn)/Ti of the oil shale samples ranges in 65.02–78.09 and 6.60–25.82, respectively, indicating that during oil shale sedimentation, the paleoclimate is warm and humid with moderate chemical weathering and that there are obviously hydrothermal fluid activities. The correlation between δCe_N and δEu_N , total rare earth elements (ΣREE) and $(Dy/Sm)_N$, implying that the diagenesis of oil shale is relatively low with middle diagenetic stage A period. The Ce_{anom} of oil shale samples ranges from -0.094 to -0.049 , suggesting that the redox condition of oil shale sedimentation is dominated by strong reducing condition, and the $(La/Yb)_n$ is from 1.3 to 2.1, manifesting the whole sedimentary rate of oil shale is relatively low. By the comparison with REEs distribution characteristics from surrounding potential provenance, the main provenances of Chang 7 sedimentation in southern Ordos Basin are from Yinshan Mountain and Qinling-Dabie Mountain.

Keywords: elements geochemistry; oil shale; Chang 7; geological implications; Ordos Basin

1. Introduction

Recent years, with the decreasing conventional petroleum, oil shale is gradually becoming one of the most significant unconventional resources and has received unprecedented attention [1–4]. Oil shale from Ordos Basin is regarded as the most typical lacustrine oil shale, from which oil shale of

Chang 7 oil layer has the features of wide distribution, abundance, shallow burial, and so on [4–11]. According to latest energy investigation, the shale oil resources of the oil shale in southern Ordos Basin have already exceeded 3500×10^8 barrels with great exploration prospective, taking up 34% of the whole shale oil resources in China [10].

The element geochemistry studies of oil shale have been a hot topic in recent years. The elements record the geological information in the shale, and can be well preserved, so it can be used to restore the palaeosedimentary environment. By the trace elements of marine oil shales from Bilong Co in northern Tibet, the elements occurrence and environment during oil shale sedimentation were discussed [12]. Wang et al. studied the trace and rare earth elements of the black shale from Wuyu Basin, and though the paleosalinity was a brackish water environment and the paleoclimate was semiarid to semimoist [13]. Qiu et al. testifies the existence of hydrothermal fluid activities of the oil shale in the southern Ordos Basin by platinum group elements [14]. In addition, the rare earth elements of oil shale can also indicate the provenance. By the comparison of rare earth elements distribution, the oil shale from the Central Eastern Desert was proved from Neoproterozoic island arc parent rocks [15]. Qiu et al. studied the rare earth elements of fine grand sediments of every sub-unit of Yanchang Formation and found that the provenance of the whole Ordos Basin changed from the Chang 7 period [16].

Oil yield and total sulfur of the oil shale from Chang 7 Formation in southern Ordos Basin showed industrial quality of middle-grade ($5\% < \text{oil yield} \leq 10\%$) with extra-low sulfur criterion (total sulfur $\leq 1.0\%$) [4,17–19]. The organic geochemistry studies indicated that most of the oil shale in the southern Ordos Basin has entered maturity [4,20]. During oil shale sedimentation, the water is dominated by fresh water, along with an average water depth of 67.01 m and the lake was proved to be an extremely eutrophic lake [5]. When considering that the studies of organic geochemistry, such as oil yield, total organic carbon (TOC), and vitrinite reflectance, are of great importance to resources calculation, the researches of inorganic geochemistry, especially major elements and rare earth elements, are still desperately inadequate, leading to many remaining unresolved issues.

In order to have a better understanding of oil shale from the Chang 7 oil layer, systematic major elements and rare earth elements characteristics, grain size analyses, and their geological implications of oil shale outcrops of the Yishicun Profile in Tongchuan City are discussed to reconstruct sedimentary background and tectonic setting for the further development of unconventional resources in China.

2. Geological Setting

Located in central China, the Ordos Basin is a Mesozoic superimposed basin that developed in the Palaeozoic North China Craton with a Proterozoic crystalline basement. As shown in Figure 1a, the basin is bounded by Hetao Basin in the north, Fenwei Graben system in the southeast, and Yinchuan Basin in the west with $25 \times 10^4 \text{ km}^2$ [21–23]. In the late Mesozoic Era, the basin started to evolved to a continental basin from North China Block with a relatively stable tectonic setting. Influenced by Indosinian orogeny, the southern Ordos basin proved to be an intracontinental foreland basin during the period of Yanchang Formation, which is dominated by fluvial-lacustrine depositional system [20,24–26]. By Early Cretaceous, the basin, especially its southern part, gradually uplifted and finally underwent reformation. According to sedimentary cycles and lithological assemblages, the Yanchang Formation is divided into ten oil layers, named as Chang 10 to Chang 1 from the bottom to the top, showing an intergrated record of progradation-aggradation-retrogradation cycle (Figure 1b) [4,5,20]. During the Chang 7 period, the basin developed the most extensive lake transgression, forming stable but unequal oil shale section.

The oil shale profile is located in Yishicun, Tongchuan City, with distinct outcrops at the bottom of the Chang 7 oil layer (Figure 1c). The whole thick of oil shale section is approximately 17 m and its occurrence is almost horizontal. The lithologies of the oil shale section are mainly oil shale and mudstone with multi-storey thin tuffs and sandstones.

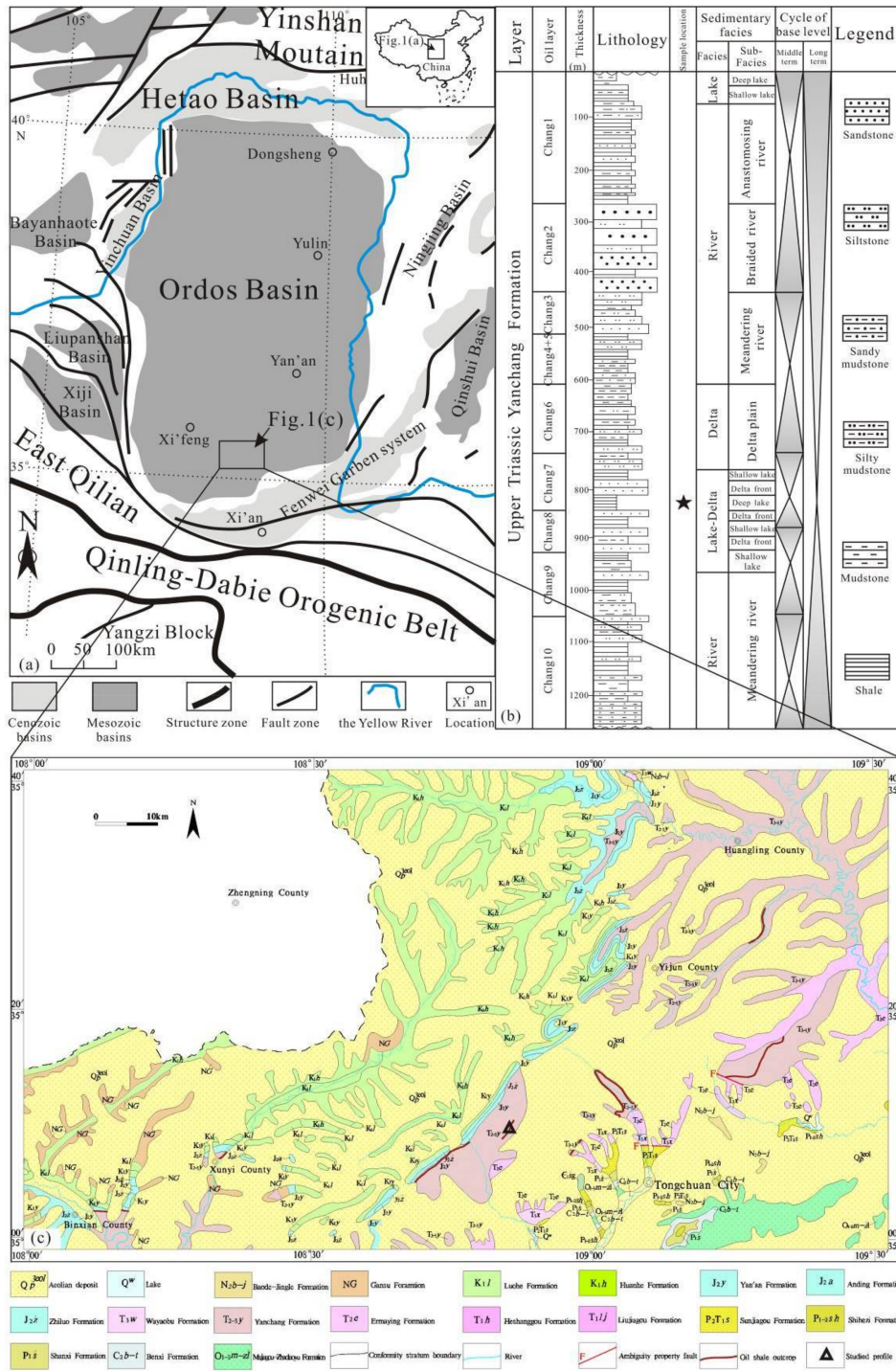


Figure 1. (a) Tectonic sketch map of Ordos Basin and adjacent areas (modified after Wang et al. [21]). (b) Stratigraphic column of Upper Triassic Yanchang Formation (modified after Li et al. [4]). (c) Simplified geological map of southern Ordos Basin (modified after Ma et al. [18] and Li et al. [4]).

3. Samples and Methods

Twelve oil shale samples and four sandstone samples were gathered from the oil shale section in Yishicun profile, Tongchuan city. Details of the rock assemblages and numbers of samples are shown in Figure 2. The four sandstone samples were all inside the oil shale seam at an equal spacing from the bottom to the top (Figure 2). Samples were collected in kraft bags prevent from contamination and oxidation.

For major elements analysis, the samples were all crushed and grounded to less than 200 mesh size and the ashed samples were sent to an open muffle furnace with the raising temperature to 950 °C. Then, the samples were dissolved in HClO₄ and HF, and the tests were conducted with X-ray fluorescence, AA-6800 atomic absorption spectroscopy, and UV-2600 ultraviolet-visible spectrophotometer. The analytical methods followed Chinese National Standard GB/T14506.1~14-2010 [27]. The analytical uncertainty was usually less than 5%.

For rare earth elements analysis, the samples were powdered to less than 200 mesh size and were digested in a microwave furnace using an HF + HNO₃ mixture in Teflon bombs at 190 °C for 48 h and were then determined with a Perkin Elmer SciexElan 6000 ICP-MS with the analysis method of Chinese National Standard GB/T14506.30-2010 [28]. The analytical error was controlled within 5%.

Sandstone samples were reduced to the known quantity by the coning and quartering method. Grain size analysis was handled with the dry sieving technique [29]. With finer than 4Φ, slice samples were analyzed using the pipette method that was described from Griffiths [30] and Carvert [31]. Various grain size parameters were computed by GRADISTAT software [32]. These analyses were conducted at National Key Laboratory of the Northwestern University, Xi'an, China.

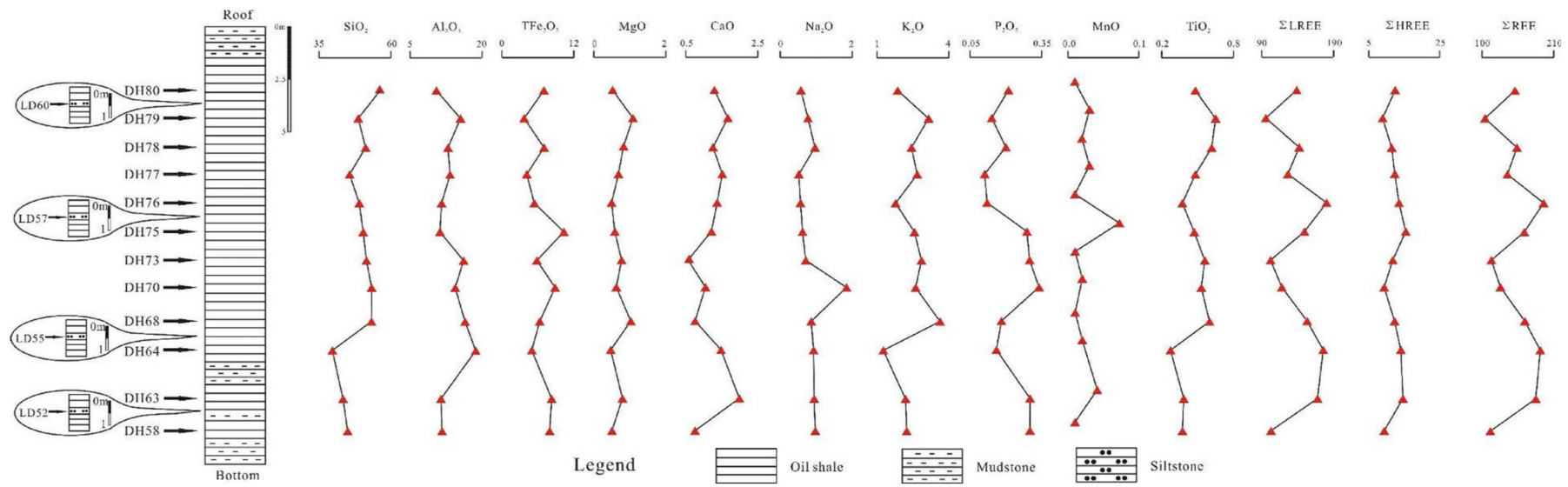


Figure 2. Vertical variation of major elements and rare earth elements of oil shale samples (unit of major elements and rare earth elements in wt % and ppm, respectively).

4. Results

4.1. Major Elements Characteristic

Table 1 listed the results for major elements of oil shale samples. The SiO_2 , Al_2O_3 , and TFe_2O_3 (total iron) abundances show the most abundant three elements (average value > 5 wt %) and the rest seven major elements are detected with the concentration being less than 5 wt % (Table 1). The whole major elements concentrations of oil shale samples vary slightly and show no obvious vertical variation rules, indicating that the heterogeneity of oil shale samples is relatively low (Figure 2). Notably, slight variations of Al_2O_3 and TiO_2 concentration can also explain that terrigenous detrital input is relatively stable (Figure 2). Element Si is mainly occurs in quartz and clay minerals in fine-grained sediments [33,34]. To some extent, the Al/Si ratio can reflect minerals in oil shale samples and the ratio gradually decreases with the increasing quartz content [4,33]. The Al/Si ratios of oil shale samples range from 0.21 to 0.36, with an average of 0.29 (Table 3, Figure 3), indicating that quartz dominates the minerals (Figure 4a), which is in accordance with the previous research using XRD analysis [5,23]. The lithology of the oil shale is classified as shale type (Figure 4b). Si/(Si + Al + Fe) ratio can offer judgment on the terrigenous provenance distance, and decreases with the increasing distance [35]. The Si/(Si + Al + Fe) of oil shale samples varies from 0.63 to 0.72, with an average of 0.67 (Table 3), indicating that the oil shale samples were formed near terrigenous provenance.

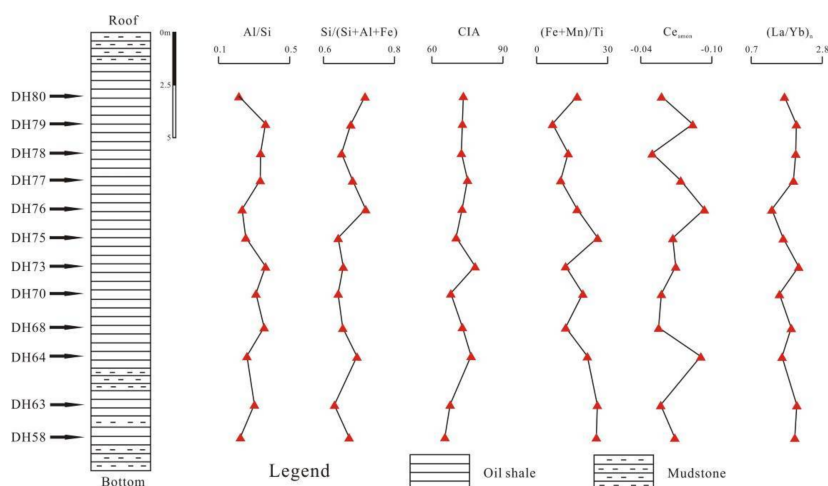


Figure 3. Vertical variation of geochemical parameters of oil shale samples.

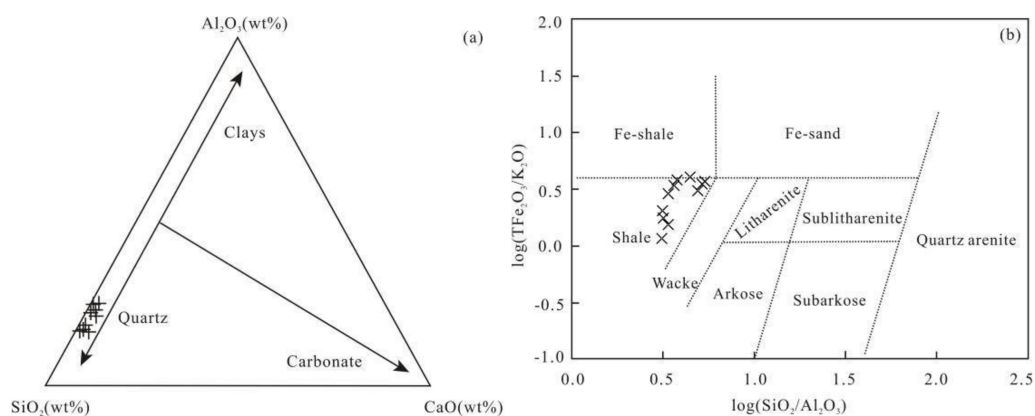


Figure 4. (a) Ternary diagram showing relative proportions of major elements (the base map is from He et al. [36]); (b) lithology classification of oil shale samples (the base map is from Herron. [37]).

Table 1. Major elements concentration in oil shale samples (unit in wt %).

Samples ID	SiO ₂	Al ₂ O ₃	TFe ₂ O ₃	MgO	CaO	Na ₂ O	K ₂ O	P ₂ O ₅	MnO	TiO ₂
DH80	56.60	10.52	6.95	0.51	1.29	0.57	1.85	0.21	0.01	0.48
DH79	48.66	15.61	3.65	1.08	1.68	0.77	3.13	0.14	0.03	0.65
DH78	51.21	14.99	7.02	0.81	1.25	0.96	2.43	0.20	0.02	0.62
DH77	45.70	13.38	4.10	0.68	1.51	0.50	2.66	0.11	0.03	0.48
DH76	48.95	9.88	5.37	0.48	1.37	0.56	1.75	0.12	0.01	0.37
DH75	50.43	11.21	10.34	0.57	1.22	0.62	2.55	0.29	0.07	0.47
DH73	51.48	16.20	5.83	0.76	0.55	0.71	2.85	0.30	0.01	0.56
DH70	53.29	14.50	8.86	0.61	1.04	1.85	2.60	0.34	0.02	0.53
DH68	53.24	16.60	6.24	1.02	0.75	0.86	3.63	0.18	0.01	0.60
DH64	39.56	8.86	4.95	0.46	1.48	0.43	1.24	0.16	0.02	0.27
DH63	43.27	11.42	8.30	0.78	1.99	0.95	2.18	0.30	0.04	0.38
DH58	45.00	8.72	8.00	0.49	0.75	0.98	2.24	0.30	0.01	0.37
Average	48.95	12.66	6.63	0.69	1.24	0.81	2.43	0.22	0.02	0.48

4.2. Rare Earth Elements Characteristic

The rare earth elements (REEs) of twelve oil shale samples are presented in Table 2. The total rare earth elements (Σ REE) of the oil shale samples are relative low (104.69–194.96 ppm, averaging 151.16 ppm), as compared to Σ REE of shale from Chang 9 oil layer in the southern Ordos Basin (average 212.35 ppm) [38]. The ratio of total light REEs (Σ LREE) to total heavy REEs (Σ HREE) varies in a small range (8.72–13.41, averaging 11.52) with relatively high value (Table 3), indicating the enrichment of LREEs and a deficit of HREEs. After being normalized by Chondrite, the distribution patterns show sloping LREEs trend and flat HREEs trends with un conspicuous Ce depletion (Figure 5a). Also, after being normalized by North American shale composite (NASC), all of the samples reveal shale like pattern [33]. The extremely unified distributing patterns of oil shale samples indicate that the REEs in the oil shale samples have been derived from the same terrigenous source and are controlled by similar sedimentary environment with almost no difference. Vertically, Σ LREE shows consistent variation with Σ REE, while the correlation between Σ HREE and Σ REE is not obvious (Figure 2). In both distribution patterns of REEs, the HREEs all display a slightly rich trend (Figure 5), which is probably influenced by the absorption of organic matter [39].

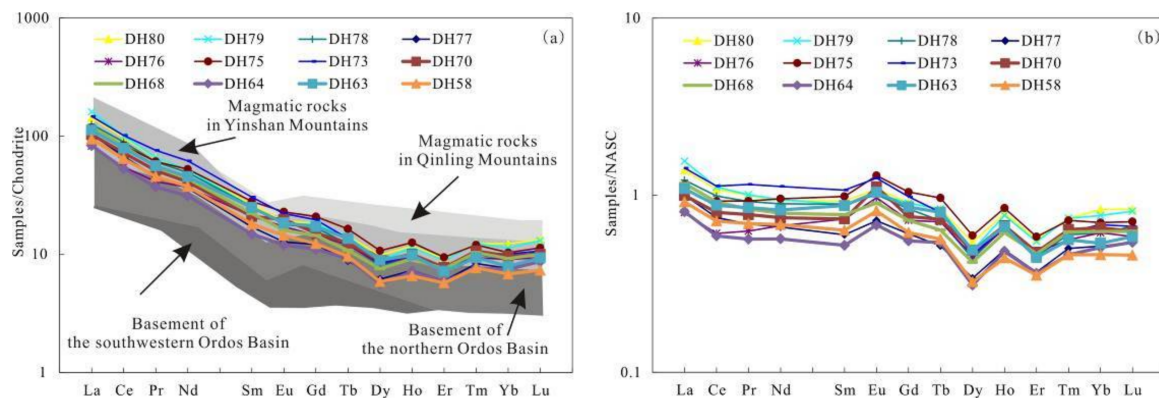


Figure 5. (a) Chondrite-normalized distribution pattern of rare earth elements (REEs) (the base map is from Qiu et al. [14]) and (b) North American shale composite (NASC)-normalized distribution pattern of REEs.

Table 2. Rare earth elements concentration in oil shale samples (unit in ppm).

Samples ID	La	Ce	Pr	Nd	Sm	Eu	Gd	Tb	Dy	Ho	Er	Tm	Yb	Lu	∑LREE	∑HREE	∑REE
DH80	44.20	78.80	7.87	30.80	5.28	1.34	4.74	0.71	3.14	0.82	1.92	0.37	2.57	0.4	168.29	14.67	182.96
DH79	49.70	81.20	7.94	31.10	5.06	1.27	4.68	0.71	2.82	0.8	1.86	0.37	2.38	0.39	176.27	14.01	190.28
DH78	38.90	72.20	7.27	29.50	5.07	1.25	4.35	0.61	2.54	0.68	1.54	0.3	1.88	0.32	154.19	12.22	166.41
DH77	32.00	54.60	5.43	21.80	3.41	0.89	3.15	0.44	1.97	0.51	1.25	0.25	1.6	0.26	118.13	9.43	127.56
DH76	25.50	44.40	4.95	22.20	4.18	1.20	3.75	0.60	2.64	0.67	1.62	0.28	1.9	0.28	102.43	11.74	114.17
DH75	36.60	67.60	7.32	31.50	5.61	1.60	5.42	0.82	3.43	0.88	1.98	0.36	2.17	0.34	150.23	15.40	165.63
DH73	45.50	82.20	9.09	37.00	6.09	1.55	5.10	0.68	2.67	0.69	1.65	0.31	2.11	0.32	181.43	13.53	194.96
DH70	31.90	58.40	6.14	24.60	4.18	1.38	3.94	0.62	2.82	0.7	1.62	0.32	2.03	0.3	126.60	12.35	138.95
DH68	37.20	66.80	6.60	26.10	4.42	1.12	3.75	0.54	2.42	0.64	1.59	0.31	1.93	0.3	142.24	11.48	153.72
DH64	25.80	43.00	4.46	18.70	2.97	0.84	2.87	0.46	1.80	0.5	1.23	0.23	1.57	0.26	95.77	8.92	104.69
DH63	34.80	64.00	6.72	27.20	4.98	1.29	4.46	0.68	2.84	0.69	1.51	0.28	1.66	0.28	138.99	12.40	151.39
DH58	29.30	52.20	5.46	22.50	3.61	1.01	3.20	0.48	1.88	0.46	1.2	0.23	1.43	0.22	114.08	9.10	123.18
Chondrite ^a	0.31	0.81	0.12	0.6	0.2	0.07	0.26	0.05	0.32	0.07	0.21	0.03	0.21	0.03	2.11	1.18	3.29
NASC ^b	32	73	7.9	33	5.7	1.24	5.2	0.85	5.8	1.04	3.4	0.5	3.1	0.48	152.84	20.37	173.21
Average	35.95	63.78	6.60	26.92	4.57	1.23	4.12	0.61	2.58	0.67	1.58	0.30	1.94	0.31	139.05	12.10	151.16

Note: ∑LREE: total content of light rare earth elements ($\sum\text{LREE} = \text{La} + \text{Ce} + \text{Pr} + \text{Nd} + \text{Sm} + \text{Eu}$); ∑HREE: total content of heavy rare earth elements ($\sum\text{HREE} = \text{Gd} + \text{Tb} + \text{Dy} + \text{Ho} + \text{Er} + \text{Tm} + \text{Yb} + \text{Lu}$); ∑REE: total content of rare earth elements ($\sum\text{REE} = \sum\text{LREE} + \sum\text{HREE}$). ^a Data cited are from Taylor and McLennan [40]; ^b Data cited are from Rudnick and Gao [41].

Table 3. Geochemical parameters of oil shale samples.

Samples ID	Al/Si	Si/(Si + Al + Fe)	ICV	CIA	Ce _{anom}	(Fe + Mn)/Ti	L/H	(La/Yb) _N	(La/Sm) _N	(Gd/Yb) _N	(La/Yb) _n	(Dy/Sm) _N	δCe _N
DH80	0.21	0.72	0.97	73.04	−0.057	16.91	11.47	11.65	5.40	1.49	1.67	0.37	1.01
DH79	0.36	0.68	0.76	72.47	−0.084	6.60	12.58	14.15	6.34	1.59	2.02	0.35	0.97
DH78	0.33	0.65	0.88	72.12	−0.049	13.24	12.62	14.02	4.95	1.87	2.00	0.31	1.02
DH77	0.33	0.68	0.71	74.70	−0.074	10.03	12.53	13.55	6.05	1.59	1.94	0.36	0.99
DH76	0.23	0.72	0.90	72.53	−0.094	16.96	8.72	9.09	3.94	1.59	1.30	0.39	0.94
DH75	0.25	0.64	1.21	69.99	−0.067	25.82	9.76	11.43	4.21	2.02	1.63	0.38	0.98
DH73	0.36	0.65	0.67	78.09	−0.070	12.16	13.41	14.61	4.82	1.95	2.09	0.27	0.96
DH70	0.31	0.64	1.02	67.61	−0.057	19.54	10.25	10.65	4.92	1.57	1.52	0.42	0.99
DH68	0.35	0.65	0.82	72.52	−0.055	12.15	12.39	13.06	5.43	1.57	1.87	0.34	1.02
DH64	0.25	0.69	0.84	76.25	−0.091	21.47	10.74	11.13	5.60	1.48	1.59	0.38	0.95
DH63	0.30	0.63	1.17	67.53	−0.057	25.59	11.21	14.20	4.51	2.17	2.03	0.36	1.00
DH58	0.22	0.67	1.32	65.02	−0.069	25.25	12.54	13.88	5.24	1.81	1.98	0.33	0.98
Average	0.29	0.67	0.94	71.82	−0.069	17.15	11.52	12.62	5.12	1.72	1.80	0.36	0.98

Note: L/H = $\sum\text{LREE}/\sum\text{HREE}$; N: chondrite-normalized; n: NASC-normalized.

4.3. Grain Size Parameters

The results of grain size analysis are shown in Table 4. The parameters of samples vary a little with mean grain size (Mz) from 3.71Φ to 4.09Φ , which means that the sandstone samples are all siltstone. The C ($2^{(\Phi_{11})} \times 1000$) and V ($2^{(\Phi_{150})} \times 1000$) range in $115.82\text{--}137.74 \mu\text{m}$ and $59.54\text{--}76.95 \mu\text{m}$. The distribution of particle size displayed one-part form with little rolling and suspension (Figure 6a), and the four samples all plot in Turbidite part (Figure 6b), suggesting that the main transport is saltation and siltstone is the turbidity event deposition results.

Table 4. Grain size analysis of four sandstone samples (units of C and M in μm , the rest units in Φ).

Sample ID	C	M	Phi1	Phi5	Phi10	Phi16	Phi25	Phi50	Phi75	Phi84	Phi90	Phi95	Mz
LD52	115.82	59.54	3.11	3.52	3.60	3.69	3.81	4.07	4.31	4.42	4.49	4.77	4.09
LD55	135.84	75.36	2.88	3.10	3.26	3.34	3.46	3.73	4.05	4.22	4.38	4.56	3.77
LD57	137.74	67.45	2.86	3.32	3.46	3.54	3.63	3.89	4.21	4.36	4.48	4.63	3.92
LD60	136.79	76.95	2.87	3.05	3.14	3.24	3.37	3.70	4.02	4.17	4.29	4.44	3.71

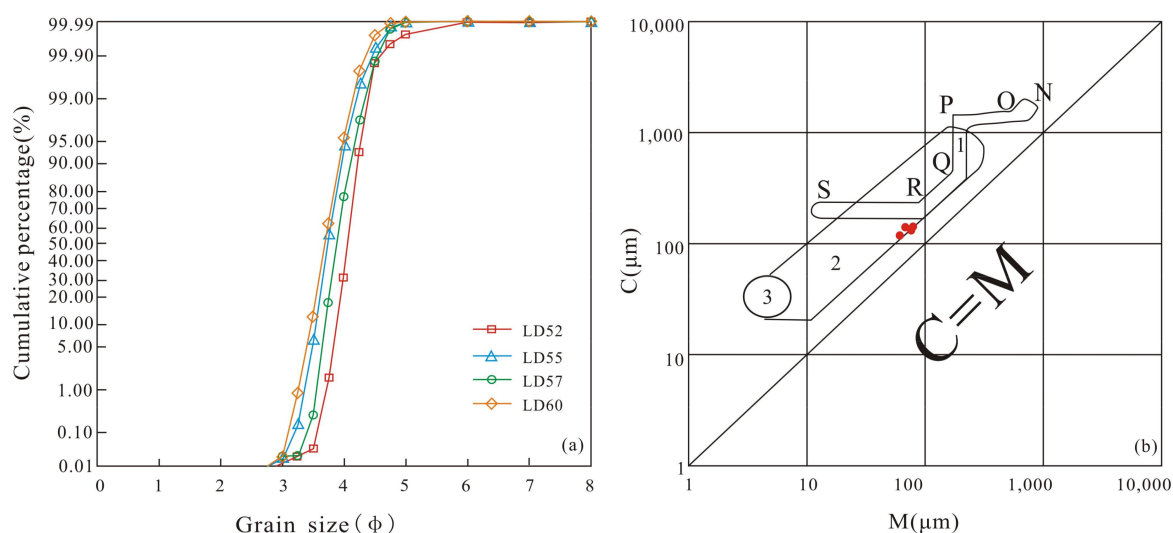


Figure 6. (a) Distribution of particle size parameters and (b) C-M pattern diagrams of sandstone samples. 1, Tractive current; 2, Turbidite; 3, Water suspension. N-O, Rolling grains; O-P, Rolling transport; P-Q, Suspension; Q-R, Graded suspension; R-S, Homogeneous suspension (the base map is from Passega [42]).

5. Discussions

5.1. Geochemistry Implications of Major Elements

5.1.1. Paleoclimate

Palaeoclimate is the climate of a certain stage in geological history and is of great significance for the resources exploration [43–46]. Chemical index of alteration (CIA) is usually adopted to reflect paleoclimate during the sedimentary period [47–49]. CIA values of 50–65, 65–85, and 85–100 indicate cold and dry with low chemical weathering, warm and humid with moderate chemical weathering, and hot and humid climate with strong chemical weathering, respectively [49], and the CIA can be calculated as follow:

$$CIA = 100 \times [Al_2O_3 / (Al_2O_3 + CaO^* + Na_2O + K_2O)]$$

where all of the oxide concentration is calculated in molecular proportions. However, when considering the change of original composition on fine grained detrital rock from recirculation deposit, index of compositional variability (ICV) should be firstly applied to judge whether experiencing recirculation deposition. The formular is:

$$\text{ICV} = (\text{Fe}_2\text{O}_3 + \text{K}_2\text{O} + \text{Na}_2\text{O} + \text{CaO}^* + \text{MgO} + \text{MnO} + \text{TiO}_2) / \text{Al}_2\text{O}_3.$$

where CaO^* represents CaO in silicate and is calculated by the expression:

$$\text{CaO}^* = \text{CaO} - (10/3) \times \text{P}_2\text{O}_5.$$

where CaO^* is the minimum between the calculated result and the Na_2O concentration.

Normally, ICV that is higher than 1 indicates more clay minerals in samples and the samples undergo less recirculation deposit. When the ICV is lower than 1, it means that the samples have less clay minerals and are affected by more sediment recycling or strong weathering [49,50]. Although the average ICV of oil shale samples is below 1, some of the samples are still over 1 and most of the other samples are very close to 1 (Table 3). Thus, it can be seen that the oil shale samples were affected by relatively weak recirculation deposit and CIA can be used to judge paleoclimate.

The CIA of oil shale samples ranges from 65.02 to 78.09 with an average of 71.82 (Table 3, Figure 3), showing that the paleoclimate is dominated by warm and humid with moderate chemical weathering during oil shale sedimentation. The ternary diagram of chemical alteration show the same observation with the CIA value (Figure 7).

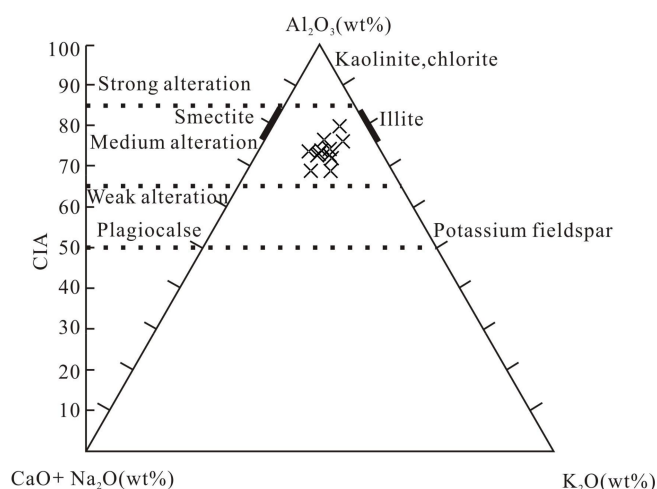


Figure 7. Ternary diagram of chemical alteration (the base map is from Li et al. [6]).

5.1.2. Hydrothermal Fluid Sedimentation

Major elements can react to hydrothermal fluid activities accurately and have been widely applied [6,35,51–53]. Usually, if the sediments were affected by hydrothermal fluid activities, $(\text{Fe} + \text{Mn})/\text{Ti}$ of sediments would be more than 15 [5,54]. As it can be seen from Table 3, the $(\text{Fe} + \text{Mn})/\text{Ti}$ of the oil shale samples varies in the range of 6.60–25.82 (average 17.15) (Figure 3), clearly manifesting that the oil shale experienced hydrothermal fluid activities. Apart from the evidence of major elements, a slightly enriched trend of HREEs has been considered to be a strong association with hydrothermal fluid activities [55]. In both normalized distribution patterns, HREEs all display an enriched trend, which can also indicate hydrothermal fluid activities (Figure 5). Besides, when compared with chondrite, an obvious high positive Eu anomaly is considered to be the presence of hydrothermal fluid [6,51–53]. As can be seen in chondrite-normalized distribution pattern of REEs, the high positive anomaly of Eu further support the hydrothermal events (Figure 5a).

Previous studies indicated that hydrothermal fluid activities mainly have two influences on organic matter [6,51]. On one hand, hydrothermal fluid can bring nutritional ingredients, such as P, Mo, and Cu, which can directly improve organic matter concentration. On the other hand, some saline material that is produced from hydrothermal fluid can facilitate organic matter preservation [6,49]. Therefore, hydrothermal fluid activities are of great importance to the formation and preservation of the high quality oil shale.

5.2. Geochemistry Implications of Rare Earth Elements

5.2.1. Diagenesis Stage

Rare earth elements can respond well to diagenesis and δCe_N is a sensitive parameter. When diagenesis is strong, δCe_N shows intense positive correlation with δEu_N and ΣREE , and negative correlation with $(Dy/Sm)_N$. On the contrary, when the diagenesis is weak, the correlation is inconspicuous [56]. As it can be seen in Figure 8, the extreme weak correlations between δCe_N and δEu_N , ΣREE , and $(Dy/Sm)_N$ illustrate the relatively weak diagenesis. Previous organic geochemistry studies on the oil shale from Yishicun Profile indicate that the type of organic matter is dominated by II_2 and the origin of organic matter are mixed with algae, phytoplankton, and terrestrial plants [4]. The R_o and T_{max} of oil shale ranges in 0.98–1.15% and 422–469 °C, with averages of 1.06% and 437.35 °C, respectively. According to the division of diagenetic stages in clastic rocks [57], the oil shale is mainly in middle diagenetic stage A period.

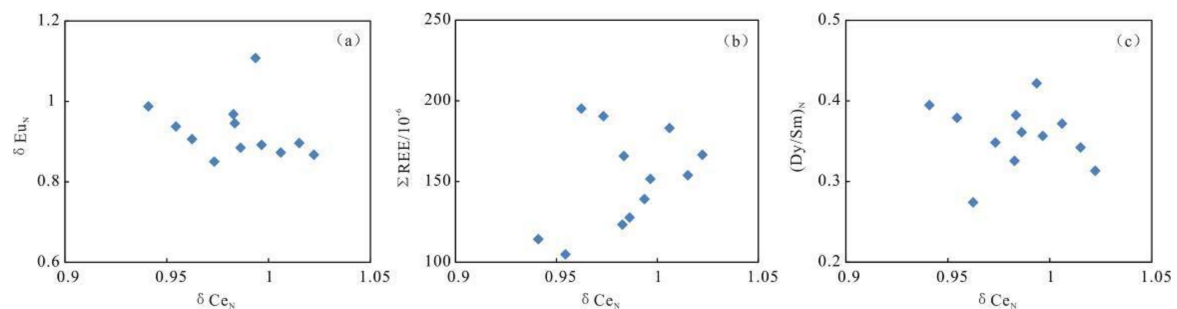


Figure 8. Relationship between δCe_N and δEu_N , total rare earth elements (ΣREE), and $(Dy/Sm)_N$ of oil shale samples.

5.2.2. Paleo Aqueous Medium

The Ce anomalies in sediments have been considered as a suitable indicator for understanding contemporaneous paleo-redox conditions [58–63]. Because of the changeable valence state of Ce, Ce could exist in the stable valence of Ce^{3+} in aqueous solution. However, Ce could be oxidized in the form of Ce^{4+} and easy to subside [64]. So, the redox condition can affect Ce anomaly, which can track ancient redox conditions [13,65]. Generally, Ce_{anom} is used to reflect redox condition. When Ce_{anom} is greater than -0.1 and less than -0.1 , it means reducing and oxidation environment, respectively [7]. The $Ce_{anom} = \lg(3Ce_n/(2 \times La_n + Nd_n))$. Subscript n represents the NASC-normalized value. Ce_{anom} of oil shale samples ranges from -0.094 to -0.049 (average -0.069) (Table 3), implying that the redox condition of oil shale sedimentation is dominated by strong reducing condition.

5.2.3. Sedimentary Rate

With the changing sedimentary environment, REEs are differentiated in electrovalence and adsorbed ability and can be perceived by detention time during sedimentation [7,66,67]. Specifically, when the detention time is short, REEs would deposit sharply and a weak exchange interaction takes place with water, showing that NASC-normalized REEs distribution pattern is flat and $(La/Yb)_n$ approaches 1. Vice versa, the $(La/Yb)_n$ deviates from 1 [7,66].

The $(La/Yb)_n$ of oil shale samples ranges from 1.3 to 2.1, with an average of 1.8 (Table 3), indicating that the whole sedimentary rate of oil shale is low. When compared with the central part of the basin, $(La/Yb)_n$ is relatively high, illustrating that although the study area is located in deep lacustrine facies, some event deposits would lead to transitory variation of the sedimentary rate. In oil shale seam, syndepositional deformation structure can also explain the relatively high sedimentary rate to some extent [4].

5.2.4. The Provenance of Oil Shale and Orogeny Coupling Response

By the diagrams of $\Sigma REE-La/Yb$, $Al_2O_3/SiO_2-(MgO + TFe_2O_3)$, and $SiO_2-\log(K_2O + Na_2O)$, the oil shale from southern Ordos Basin has been proved to originate from felsic rocks and deposits in the continental island arc tectonic setting. Hence, in this contribution, there is no further discussion on the parent rock and tectonic setting of the oil shale [7]. However, due to complex orogeny during the Chang 7 period, the source direction of sediments is still discussed controversially. Massive detrital minerals indicate that there are two similar sedimentary periods in the Yanchang Formation [68]. One is Chang 10–Chang 8 and the other one is Chang 7–Chang 1. The source of conversion period between Chang 8 and Chang 7 is changed, referring the possible provenance of southern Ordos Basin in Chang 7 period. However, average element geochemistry data of individual samples in the southern Ordos Basin reveals that Yinshan Mountain, which locates the north of the Ordos Basin, provided provenance to the whole basin in Chang 9–Chang 7 period without northern provenance [19]. While in Chang 6–Chang 3 period, Qinlin-Dabie, which is located to the south of the Ordos Basin, started to offer provenance to southern Ordos Basin. Therefore, it is certain that the northern Yinshan Mountain provided provenance to the whole basin. Whether there was a source in southern Ordos Basin during Chang 7 period is not clear and this is of great importance to the sedimentary environment and the tectonic response. However, due to the sensitive and stable characteristics of REEs, REEs can be indicators for sedimentary and orogeny response and can explain this issue well.

As discussed in Section 4.2, the Chondrite-normalized distribution pattern of REEs of oil shale samples shows a sloping LREEs trend and flat HREEs trends. The pattern plots present two different kinds of provenances (Figure 5a), indicating that the source of Chang 7 is mixed. One source comes from magmatic rocks in Yinshan Mountain and the other one stems from the basement of the northern Ordos Basin.

The southern Ordos Basin is adjacent to the Qinling-Dabie Orogenic Belt and East Qilian. During the Chang 7 period, the Yangtze plate collided the North China Block with Qinling orogeny. Thus, the collision orogeny and uplift denudation affected tectonic, depositional background, and the source of sediments [21]. Also, the zircon SHRIMP U–Pb age of laminated tuff in southern basin founded that the tuff was from the Qinling-Dabie Orogenic Belt in $230 \text{ Ma} \pm$ [69], which demonstrates that the Qinling-Dabie Mountain has the possibility of providing source for the southern basin both in time and space. In addition, Li et al. [4] found that the organic matter type of the oil shale in the studied profile is dominated by Type II₂ and the source of organic matter is mixed with algae, phytoplankton, and terrestrial plants. While, previous recognitions demonstrated that the organic matter type of oil shale in the basin center is mainly Type I with little terrestrial plants and oil shale in whole basin all deposits in semi-deep to deep lake [4,70,71]. So, the only reasonable explanation for the above abnormal phenomena in oil shale must be attributed to Qinling orogeny, which brought a considerable amount of terrestrial plants to the southern paleolake, accompanied with turbidite events. All of these researches can also be one of the responsive evidence on the other side, which is in accordance with the results of $Si/(Si + Al + Fe)$, as well.

Therefore, the REEs of the oil shale samples exactly reflect that the provenance of Chang 7 oil layer in southern Ordos Basin comes from both Yinshan Mountain and Qinling-Dabie Mountain.

6. Conclusions

This paper presents a systematic research on major elements, rare earth elements characteristics, grain size analysis, and the geological implications of an oil shale section from the Chang 7 oil layer in southern Ordos Basin. Based on the above experimental results, the following conclusions can be obtained:

(1) Al/Si and Si/(Si + Al + Fe) of oil shale samples from Chang 7 oil layer in southern Ordos Basin indicate that quartz is dominated in minerals and the oil shale deposits near terrigenous provenance. $\Sigma\text{LREE}/\Sigma\text{HREE}$ of the shale samples varies in the range of 8.72–13.41, suggesting the enrichment of LREEs and the deficit of HREEs. The Chondrite- and NASC-normalized patterns show that the oil shale has been derived from the same terrigenous source and is controlled by a similar sedimentary environment. The sandstone lithology is mainly siltstone caused by turbidity sediment possibly.

(2) CIA of oil shale samples ranges from 65.02 to 78.09, indicating that the paleoclimate during oil shale sedimentation is mainly warm and humid with moderate chemical weathering. $(\text{Fe} + \text{Mn})/\text{Ti}$ of oil shale samples is in the range of 6.60–25.82, with an average of 17.15, implying that there are obviously hydrothermal fluid activities during the formation of oil shale.

(3) The diagenetic stage stays in middle diagenetic stage a period. The redox condition of paleo aqueous medium is a strong reducing condition. The whole sedimentary rate of oil shale is relatively low. The sedimentary rate may have been associated with some event deposits.

(4) In the Chang 7 period, there should be two main provenances existing in the southern Ordos Basin. One is Yinshan Mountain, to the north of Ordos Basin; the other one is Qinling-Dabie Mountain, to the southern Ordos Basin.

Acknowledgments: Authors would like to thank the financial support from the National Natural Science Foundation of China (No. 41173055; No. 41772118) and the Fundamental Research Funds for the Central Universities (No. 310827172101). We are grateful to Wei Zhou of Chang'an University for the constructive comments, which improved this paper greatly.

Author Contributions: Delu Li and Rongxi Li conceived and designed the experiments, corrected the draft intensively, submitted the paper and pay for the processing fees; Delu Li, Futian Liu, Bangsheng Zhao, Di Zhao performed the experiments, analyzed the data and wrote the drafts of the paper; Tao Xue and Baoping Wang helped in the preparation of the paper and in checking the drafts of the paper.

Conflicts of Interest: The authors declare no conflict of interest.

References

1. Hakimi, M.H.; Wan, H.A.; Alqudah, M.; Makeen, Y.M.; Mustapha, K.A. Organic geochemical and petrographic characteristics of the oil shales in the Lajjun area, Central Jordan: Origin of organic matter input and preservation conditions. *Fuel* **2016**, *181*, 34–45. [[CrossRef](#)]
2. Song, Y.; Liu, Z.; Meng, Q.; Xu, J.; Sun, P.; Cheng, L.; Zheng, G. Multiple controlling factors of the enrichment of organic matter in the upper cretaceous oil shale sequences of the Songliao Basin, NE China: Implications from geochemical analyses. *Oil Shale* **2016**, *33*, 142–166. [[CrossRef](#)]
3. Lv, D.W.; Li, Z.X.; Liu, H.Y.; Li, Y.; Feng, T.T.; Wang, D.D.; Wang, P.L.; Li, S.Y. The characteristics of coal and oil shale in the coastal sea areas of Huangxian Coalfield, Eastern China. *Oil Shale* **2015**, *32*, 204–207. [[CrossRef](#)]
4. Li, D.; Li, R.; Zhu, Z.; Wu, X.; Cheng, J.; Liu, F.; Zhao, B. Origin of organic matter and paleo-sedimentary environment reconstruction of the Triassic oil shale in Tongchuan City, Southern Ordos Basin (China). *Fuel* **2017**. [[CrossRef](#)]
5. Li, D.; Li, R.; Zhu, Z.; Wu, X.; Liu, F.; Zhao, B.; Cheng, J.; Wang, B. Elemental characteristics and paleoenvironment reconstruction: A case study of the Triassic lacustrine Zhangjiatan oil shale, southern Ordos Basin, China. *Acta Geochim.* **2017**. [[CrossRef](#)]
6. Li, D.; Li, R.; Zhu, Z.; Wu, X.; Liu, F.; Zhao, B.; Wang, B. Influence on lacustrine source rock by hydrothermal fluid activities—a case study of oil shale from Chang 7 Oil layer in southern Ordos Basin. *Acta Geochim.* **2017**. [[CrossRef](#)]

7. Li, D.; Li, R.; Zhu, Z.; Wu, X.; Zhao, B.; Cheng, J.; Liu, F. Rare earth elements geochemistry characteristics and their geological implications of lacustrine oil shale from Chang 7 oil layer in southern Ordos Basin, China. *Geol. J.* **2017**. [[CrossRef](#)]
8. Bai, Y.L.; Ma, L.; Wu, J.W.; Ma, Y.H. Geological characteristics and resource potential of oil shale in Ordos Basin. *Geol. China* **2009**, *36*, 1123–1137. (In Chinese)
9. Zhang, Q.C.; Wang, K.M.; Luo, S.S.; Wu, X.Z. Study on the Characteristics and Origin of the Oil Shale in the Chang 7 Member, Yanchang Formation in Ordos Basin. *Adv. Geosci.* **2013**, *3*, 197–209. (In Chinese) [[CrossRef](#)]
10. Luo, Y.S.; Zhang, X.N.; Zhang, Z.H.; Deng, N.T.; He, Y.H.; Liang, Q.S. Favorable area forecast of oil shale exploration in southern Ordos basin. *China Min. Mag.* **2014**, *23*, 83–86. (In Chinese)
11. Deng, N.T.; Zhang, Z.H.; Ren, L.Y.; Wang, F.B.; Liang, Q.S.; Li, Y.X.; Li, W.H.; Zhao, S.F.; Luo, M.J. Geochemical characteristics and distribution rules of oil shale from Yanchang Formation, Southern Ordos Basin. *Pet. Geol. Exp.* **2013**, *35*, 432–437. (In Chinese)
12. Fu, X.; Jian, W.; Tan, F.; Feng, X.; Zeng, S. The geochemistry of trace elements in marine oil shales and their combustion residues: Occurrence and environmental aspects. *Energy Sources* **2016**, *38*, 410–419. [[CrossRef](#)]
13. Wang, Z.; Fu, X.; Feng, X.; Song, C.; Wang, D.; Chen, W.; Zeng, S. Geochemical features of the black shales from the Wuyu Basin, southern Tibet: Implications for palaeoenvironment and palaeoclimate. *Geol. J.* **2017**, *52*, 282–297. [[CrossRef](#)]
14. Qiu, X.; Liu, C.; Mao, G.; Deng, Y.; Wang, F.; Wang, J. Major, trace and platinum-group element geochemistry of the Upper Triassic nonmarine hot shales in the Ordos basin, Central China. *Appl. Geochem.* **2015**, *53*, 42–52. [[CrossRef](#)]
15. Fathy, D.; Wagreich, M.; Zaki, R.; Mohamed, R.S.A.; Gier, S. Geochemical fingerprinting of maastrichtian oil shales from the central eastern desert, egypt: Implications for provenance, tectonic setting, and source area weathering. *Geol. J.* **2017**, 1–16. [[CrossRef](#)]
16. Qiu, X.W.; Liu, C.Y.; Wang, F.F.; Deng, Y.; Mao, G.Z. Trace and rare earth element geochemistry of the Upper Triassic mudstones in the southern Ordos Basin, Central China. *Geol. J.* **2015**, *50*, 399–413. [[CrossRef](#)]
17. Sun, S.S.; Yao, Y.B.; Lin, W. Elemental Geochemical Characteristics of the Oil Shale and the Paleolake Environment of the Tongchuan Area, Southern Ordos Basin. *Bull. Miner. Petrol. Geochem.* **2015**, *34*, 642–645. (In Chinese)
18. Ma, Z.H.; Chen, Q.S.; Shi, Z.W.; Wang, C.; Du, W.G.; Zhao, C.Y. Geochemistry of oil shale from Chang 7 reservoir of Yanchang Formation in south Ordos Basin and its geological significance. *Geol. Bull. China* **2016**, *35*, 1550–1558. (In Chinese)
19. Yang, H.; Niu, X.B.; Xu, L.M.; Feng, S.B.; You, Y.; Liang, X.W.; Wang, F.; Zhang, D.D. Exploration potential of shale oil in Chang7 Member, Upper Triassic Yanchang Formation, Ordos Basin, NW China. *Pet. Explor. Dev.* **2016**, *43*, 511–520. (In Chinese) [[CrossRef](#)]
20. Li, D.; Li, R.; Wang, B.; Liu, Z.; Wu, X.; Liu, F.; Zhao, B. Study on oil-source correlation by analyzing organic geochemistry characteristics: A case study of the Upper Triassic Yanchang Formation in the south of Ordos Basin, China. *Acta Geochim.* **2016**, *35*, 1–13. [[CrossRef](#)]
21. Wang, J.Q.; Liu, C.Y.; Guo, Z.; Zhang, D.D. Sedimentary response of regional tectonic transformation in Late Triassic Yanchang period at the central and southern Ordos Basin. *Earth Sci. Front.* **2015**, *22*, 194–204. (In Chinese)
22. Wan, Y.S.; Xie, H.Q.; Yang, H.; Wang, A.J.; Liu, D.Y.; Kröner, A.; Wilde, S.A.; Geng, Y.S.; Sun, L.Y.; Ma, M.Z.; et al. Is the Ordos block Archean or Paleoproterozoic in age? Implications for the Precambrian evolution of the North China craton. *Am. J. Sci.* **2013**, *313*, 683–711. [[CrossRef](#)]
23. Wang, X.F. *Non-Seismic Oil and Gas Exploration in Ordos Basin*; Geological Publishing House: Beijing, China, 1992. (In Chinese)
24. Liu, S.F. The coupling mechanism of basin and orogen in the western Ordos basin and adjacent regions of China. *J. Asian Earth Sci.* **1998**, *16*, 369–383. [[CrossRef](#)]
25. Liu, S.; Yang, S. Upper Triassic-Jurassic sequence stratigraphy and its structural controls in the western Ordos basin, China. *Basin Res.* **2000**, *12*, 1–18. [[CrossRef](#)]
26. Qiu, X.W.; Liu, C.Y.; Mao, G.Z.; Deng, Y.; Wang, F.F. Enrichment feature of thorium element in tuff interlayers of Upper Triassic Yanchang Formation in Ordos Basin, China. *Geol. Bull. China* **2010**, *29*, 1185–1191. (In Chinese)

27. *Methods for Chemical Analysis of Silicate Rocks*; GB/T14506.1~14-2010; Standards Press of China: Beijing, China, 2010. (In Chinese)
28. *Methods for Chemical Analysis of Silicate Rocks-Part 30: Determination of 44 Elements*; GB/T14506.30-2010; Standards Press of China: Beijing, China, 2010. (In Chinese)
29. Folk, R.L. *Petrology of Sedimentary Rocks*; Hemphills Publ Co.: Austin, TX, USA, 1980; p. 170.
30. Griffiths, J.C. Size versus sorting in Caribbean sediments. *J. Geol.* **1951**, *59*, 211–243. [[CrossRef](#)]
31. Calvert, S.E.; Pedersen, T.F.; Karlin, R.E. Geochemical and isotopic evidence for post-glacial palaeoceanographic changes in Saanich Inlet, British Columbia. *Mar. Geol.* **2001**, *174*, 287–305. [[CrossRef](#)]
32. Blott, S.J.; Pye, K. GRADISTAT: A grain size distribution and statistics package for the analysis of unconsolidated sediments. *Earth Surface Process. Landf.* **2001**, *26*, 1237–1248. [[CrossRef](#)]
33. Fu, X.; Wang, J.; Zeng, Y.; Tan, F.; Chen, W.; Feng, X. Geochemistry of rare earth elements in marine oil shale—A case study from the Bilong Co area, Northern Tibet, China. *Oil Shale* **2010**, *27*, 194–208. [[CrossRef](#)]
34. Fu, X.; Wang, J.; Zeng, Y.; Tan, F.; Feng, X. REE geochemistry of marine oil shale from the Changshe Mountain area, northern Tibet, China. *Int. J. Coal Geol.* **2010**, *81*, 191–199. [[CrossRef](#)]
35. Chen, J.F.; Sun, X.L. Preliminary study of geochemical characteristics and formation-of organic matter rich stratigraphy of Xiamaling-Formation of later Proterozoic in North China. *Natl. Gas Geosci.* **2004**, *15*, 110–114. (In Chinese)
36. He, C.; Ji, L.; Wu, Y.; Wu, Y.; Ao, S.; Zhang, M. Characteristics of Hydrothermal Sedimentation Process in the Yanchang Formation, South Ordos Basin, China: Evidence from Element Geochemistry. *Sediment. Geol.* **2016**, *345*, 33–41. [[CrossRef](#)]
37. Herron, M.M. Geochemical classification of terrigenous sands and shales from core or log data. *J. Sediment. Res.* **1988**, *58*, 820–829.
38. Wang, D.Y.; Xin, B.S.; Yang, H.; Fu, J.H.; Yao, J.L.; Zhang, Y. Zircon SHRIMP U-Pb age and geological implications of tuff at the bottom of Chang-7 Member of Yanchang Formation in the Ordos Basin. *Sci. China Earth Sci.* **2014**, *44*, 2160–2171. [[CrossRef](#)]
39. Tu, Q.J.; Xu, S.Q. The REE Geochemistry of the Lucaogou Formation in the Southern Junggar Basin and Analysis of Parent Rock and Tectonic Setting in Sediment-source Region. *Xin Jiang Geol.* **2016**, *34*, 345–349. (In Chinese)
40. Taylor, S.R.; McLennan, S.M. The geochemical evolution of the continental crust. *Rev. Geophys.* **1995**, *33*, 293–301. [[CrossRef](#)]
41. Rudnick, R.; Gao, S. 4.1-Composition of the Continental Crust. *Treat. Geochem.* **2014**, *4*, 1–64.
42. Passega, R. *Texture as Characteristic of Clastic Deposition*; University of Cambridge: Cambridge, UK, 1957.
43. Madhavaraju, J. Chapter 8-Geochemistry of Late Cretaceous Sedimentary Rocks of the Cauvery Basin, South India: Constraints on Paleoweathering, Provenance, and End Cretaceous Environments. *Chemostratigraphy* **2015**, 185–214. [[CrossRef](#)]
44. Madhavaraju, J.; Tom, M.; Lee, Y.I.; Balaram, V.; Ramasamy, S.; Carranza-Edwards, A.; Ramachandran, A. Provenance and tectonic settings of sands from Puerto Peñasco, Desemboque and Bahia Kino beaches, Gulf of California, Sonora, Mexico. *J. S. Am. Earth Sci.* **2016**, *71*, 262–275. [[CrossRef](#)]
45. Mondal, M.E.A.; Wani, H.; Mondal, B. Geochemical signature of provenance, tectonics and chemical weathering in the Quaternary flood plain sediments of the Hindon River, Gangetic plain, India. *Tectonophysics* **2012**, *566–567*, 87–94. [[CrossRef](#)]
46. Ramachandran, A.; Madhavaraju, J.; Ramasamy, S.; Lee, Y.I.; Rao, S.; Chawngthu, D.L.; Velmurugan, K. Geochemistry of Proterozoic clastic rocks of the Kerur Formation of Kaladgi-Badami Basin, North Karnataka, South India: Implications for paleoweathering and provenance. *Turk. J. Earth Sci.* **2016**, *25*, 126–144. [[CrossRef](#)]
47. Young, G.M.; Nesbitt, H.W. Paleoclimateology and Provenance of the glaciogenic Gowganda Formation (Paleoproterozoic), Ontario, Canada: A chemostratigraphic approach. *GSA Bull.* **1999**, *111*, 264–274. [[CrossRef](#)]
48. Feng, L.; Chu, X.; Zhang, Q.; Zhang, T.; Li, H.; Jiang, N. New evidence of deposition under cold climate for the Xieshuihe Formation of the Nanhua System in northwestern Hunan, China. *Sci. Bull.* **2004**, *49*, 1420–1427. [[CrossRef](#)]

49. Li, D.; Li, R.; Zhu, Z.; Xu, F. Elemental characteristics of lacustrine oil shale and its controlling factors of palaeo-sedimentary environment on oil yield a case from Chang 7 oil layer of Triassic Yanchang Formation in southern Ordos Basin. *Acta Geochim.* **2017**. [[CrossRef](#)]
50. Cullers, R.L.; Podkovyrov, V.N. Geochemistry of the Mesoproterozoic Lakhanda shales in southeastern Yakutia, Russia: Implications for mineralogical and provenance control, and recycling. *Precambrian Res.* **2000**, *104*, 77–93. [[CrossRef](#)]
51. He, C.; Ji, L.M.; Su, A.; Liu, Y.; Li, J.F.; Wu, Y.D.; Zhang, M.Z. Relationship between hydrothermal sedimentation process and source rock development in the Yanchang Formation, southern Ordos Basin. *Earth Sci. Front.* **2017**. [[CrossRef](#)]
52. Michard, A.; Albarede, F.; Michard, G.; Minister, J.F.; Charlow, J.L. Rare earth elements and uranium in high temperature solutions from East-Pacific rise hydrothermal vent field (13°N). *Nature* **1983**, *303*, 795–797. [[CrossRef](#)]
53. Sherrell, R.M.; Field, M.P.; Ravizza, G. Uptake and fractionation of rare earth elements on hydrothermal plume particles at 945' N, East Pacific Rise. *Geochim. Cosmochim. Acta* **1999**, *63*, 1709–1722. [[CrossRef](#)]
54. Chu, C.L.; Chen, Q.L.; Zhang, B.; Shi, Z.; Jiang, H.J.; Yang, X. Influence on Formation of Yuertusi Source Rock by Hydrothermal Activities at Dongergou Section, Tarim Basin. *Acta Sedimentol. Sin.* **2016**, *34*, 803–810. (In Chinese)
55. Jia, Z.B.; Hou, D.J.; Sun, D.Q.; Huang, Y.X. Hydrothermal sedimentary discrimination criteria and its coupling relationship with the source rocks. *Natl. Gas Geosci.* **2016**, *27*, 1025–1034. (In Chinese)
56. Shields, G.; Stille, P. Diagenetic constraints on the use of cerium anomalies as paleoseawater redox proxies: An isotope and REE study of Cambrian phosphorites. *Chem. Geol.* **2001**, *175*, 29–48. [[CrossRef](#)]
57. *The Division of Diagenetic Stages in Clastic Rocks*; SY/T 5477-2003; Standards Press of China: Beijing, China, 2003. (In Chinese)
58. German, C.R.; Elderfield, H. Application of Ce anomaly as a paleo redox indicator: The ground rules. *Paleoceanography* **1990**, *5*, 823–833. [[CrossRef](#)]
59. Grandjean, P.; Cappetta, H.; Albarède, F. The REE and Nd of 40–70 Ma old fish debris from the West-African platform. *Geophys. Res. Lett.* **1988**, *15*, 389–392. [[CrossRef](#)]
60. Grandjean, P.; Cappetta, H.; Michard, A.; Albarede, F. The assessment of REE patterns and ¹⁴³Nd/¹⁴⁴Nd ratios in fish remains. *Earth Planet. Sci. Lett.* **1987**, *84*, 181–196. [[CrossRef](#)]
61. Liu, Y.G.; Miah, M.R.U.; Schmitt, R.A. Cerium: A chemical tracer for paleo-oceanic redox conditions. *Geochim. Cosmochim. Acta* **1988**, *52*, 1361–1371. [[CrossRef](#)]
62. Madhavaraju, J.; Loser, H.; Lee, Y.I.; Santacruz, R.L.; Pi-Puig, T. Geochemistry of Lower Cretaceous limestones of the Alisitos Formation, Baja California, Mexico: Implications for REE source and paleo-redox conditions. *J. S. Am. Earth Sci.* **2016**, *66*, 149–165. [[CrossRef](#)]
63. Madhavaraju, J.; Loser, H.; Scott, R.W.; Sandeep, S.; Sial, A.N.; Ramasamy, S. Petrography, geochemistry and stable isotopes of carbonate rocks, Lower Cretaceous Alisitos Formation, Los Torotes section, Baja California, Mexico. *Rev. Mex. Cienc. Geol.* **2017**, *34*, 63–77. [[CrossRef](#)]
64. Chen, B.H.; Wei, H.X.; Huang, Z.G.; Zhou, Y.Z. Cerium anomalies in supergene geological bodies and its effecting factors. *Chin. Rare Earths* **2007**, *28*, 79–83. (In Chinese)
65. Peng, X.F.; Wang, L.J.; Jiang, L.P. Geochemical Characteristics of the Lucaogou Formation Oil Shale in the Southeastern Margin of the Junggar Basin and Its Environmental Implications. *Bull. Mineral. Petrol. Geochem.* **2012**, *31*, 121–127. (In Chinese)
66. Wang, G.; Chen, H.; Zhu, Z.; Lin, L.; Fan, Y. The characteristics and geological implications of rare earth elements in sandstone of lower Silurian Xiaoheba Formation in the southeastern Sichuan-western Hunan. *Petrol. Geol. Exp.* **2010**, *32*, 487–495. (In Chinese)
67. Li, S.J.; Xiao, K.H.; Wo, Y.J.; Long, S.X.; Cai, L.G. REE Geochemical Characteristics and Their Geological Signification in Silurian, West of Hunan Province and North of Guizhou Province. *Geoscience* **2008**, *22*, 273–280. (In Chinese)
68. Wang, J.Q.; Liu, C.Y.; Li, X.; Wu, T.T.; Wu, J.L. Geochronology, Potential Source and Regional Implications of Tuff Intervals in Chang-7 Member of Yanchang Formation, South of Ordos Basin. *Acta Sedimentol. Sin.* **2017**, *35*, 692–704. [[CrossRef](#)]

69. Wang, X.X.; Zheng, R.C.; Yan, G.Q.; Wang, C.Y.; Chen, H.R. The Mudstone Sedimentary Environment and Provenance Analysis Based on the Geochemical Evidence of Rare Earth Elements: Take Chang 9 Oil-bearing Layer in Longdong Area of Ordos Basin as an Example. *Natl. Gas Geosci.* **2014**, *25*, 1387–1394. (In Chinese)
70. Yang, H.; Zhang, W.Z. Leading effect of the Seventh Member high-quality source rock of Yanchang Formation in Ordos Basin during the enrichment of low-penetrating oil-gas accumulation: Geology and geochemistry. *Geochimica* **2005**, *34*, 147–154. (In Chinese)
71. Zhang, W.Z.; Yang, H.; Yang, Y.H.; Kong, Q.F.; Wu, K. Petrology and element geochemistry and development environment of Yanchang Formation Chang-7 high quality source rocks in Ordos Basin. *Geochimica* **2008**, *37*, 59–64.



© 2018 by the authors. Licensee MDPI, Basel, Switzerland. This article is an open access article distributed under the terms and conditions of the Creative Commons Attribution (CC BY) license (<http://creativecommons.org/licenses/by/4.0/>).